Wear Behavior of Martensitic Stainless Steel in Rolling-Sliding Contact for Planetary Roller Screw Mechanism: Study of the WC/C Solution

Article *in* Tribology Online · April 2016

DOI: 10.2474/trol.11.209

CITATIONS
12

READS
187

4 authors, including:

V. Fridrici
Laboratoire de Tribologie et Dynamique des Systèmes
71 PUBLICATIONS **795** CITATIONS

SEE PROFILE

Ph. Kapsa
Ecole Centrale de Lyon
212 PUBLICATIONS **4,652** CITATIONS

SEE PROFILE

Tribology Online
Japanese Society of Tribologists

Tribology Online, 11, 2 (2016) 209-217.
ISSN 1881-2198
DOI 10.2474/trol.11.209

Article

Wear Behavior of Martensitic Stainless Steel in Rolling-Sliding Contact for Planetary Roller Screw Mechanism: Study of the WC/C Solution

Gilles Aurégan[1)2)*], Vincent Fridrici[1)], Philippe Kapsa[1)] and Fernand Rodrigues[2)]

[1)]Laboratoire de Tribologie et Dynamique des Systèmes (LTDS), UMR CNRS 5513 ECL-ENISE
Ecole Centrale de Lyon - Université de Lyon Bat. H10 36 avenue Guy de Collongue - 69134 Ecully cedex, France
[2)]Messier-Bugatti-Dowty, SAFRAN group, France
[*]Corresponding author: gilles.auregan@ec-lyon.fr

(Manuscript received 27 October 2015; accepted 14 January 2016; published 30 April 2016)
(Presented at the International Tribology Conference Tokyo 2015, 16-20 September, 2015)

The planetary roller screw mechanism is used in the aeronautics industry for electro-mechanical actuators application. It transforms a rotational movement into a translation movement, and it is designed for heavy loads. The main components are made of martensitic stainless steel, and lubricated with grease. Like most usual rolling mechanisms, smearing and jamming can occur before the theoretical fatigue lifetime, especially in poor lubrication conditions. The actuated load is carried by small contacts between the threads of the screw, the rollers and the nut. The static single contact can be described as an ellipsoid on flat contact with high contact pressure (3-4 GPa). The motion consists of rolling with spin associated with side slip up to 10%. The aim of our study is to investigate the wear behavior of the WC/C coated contact for different operating and design parameters such as load, speed and slip ratio. The contact is simulated by a free rolling roller loaded on a rotating disk. A specific apparatus is used to create a contact with a side slip component, i.e. perpendicular to the rolling direction. The wheel rolling speed and the tangential force generated by the slip ratio are measured. The wear behavior of a WC/C carbon-based composite coating is investigated. It reveals progressive wear and cracking in the rolling direction, i. e. perpendicular to the sliding direction. A wear map has been drawn to establish the damage mode depending on the contact conditions.

Keywords: planetary roller screw, rolling-sliding, WC/C coating, fatigue, abrasion

1. Introduction

The planetary roller screw (PRS) is a device that converts rotation to translation motion or vice versa. This mechanism includes rollers between the screw and the nut to limit friction (Fig. 1). The basic principle is similar to the ball screw mechanism, but it is designed for high speed and long lifetime applications. Especially, the rollers threads increase the contact surface and then allow carrying heavier loads for a relatively small external diameter. These features make the PRS attractive for aeronautics electro-mechanical actuators that must be small sized and highly stressed.

The lifetime calculation of this component is based on fatigue failure like most bearing mechanisms. However, it is known that bearing parts made of stainless steel often fail before the calculated time, because of other failure modes such as adhesive wear [1]. Smearing damage is closely linked to the lubrication conditions and the contact stresses, and is complicated to predict. Also, the design of PRS is quite different from usual rolling components, and includes rolling-sliding motion and parasite forces that can drastically influence the lifetime.

These particular features make the use of liquid lubricant not reliable enough to protect the surfaces from smearing. It appeared indeed that grease might be ejected from the contact sides due to the side-slip component. Hard composite coatings such as tungsten-carbide / DLC (WC/C) are studied as a solution to enhance the lifetime prediction of the PRS single contacts.

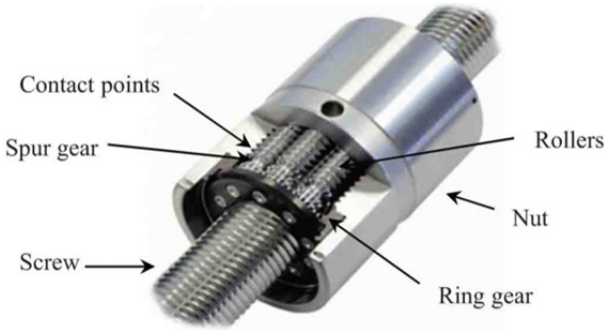

Fig. 1 PRS main components

Despite its importance in many application fields such as manufacturing and robotics, the use of the PRS never required a high level of reliability in high stress conditions. Then, very few fundamental researches have been performed to improve the design and the lifetime calculation. Yet, as the PRS becomes interesting for critical application like actuators for the aeronautics, some work has been made in recent years to better understand its kinematics [2,3].

The present work investigates the tribological behavior of the PRS mechanism with coated surfaces. First, a theoretical analysis of the contact conditions is provided. Then, a specific tribometer that reproduces the RPS contact is presented. Rolling-sliding wear tests were performed with different working conditions such as normal load, speed, and creep ratio. Results should provide tools to predict the hazardous configurations and increase the reliability.

2. Mechanical and tribological features of the contact

2.1. Static description of the contact

The PRS consists of a screw and a threaded nut of the same pitch (Fig. 1), with rollers in between. The thread profile of the screw and the nut are straight and usually cut to 90° for best efficiency. Threaded rollers are set between the two components, and their profile is curved to further reduce friction. The axial load is transmitted through multiple contacts between the threaded components. Then, these contacts can be described as ellipsoid-on-flat contacts (Fig. 2) that are characterized by three radii: the pitch radius of the screw (or the nut) and the roller, and the roller's radius of curvature. They are subjected to a single normal force F_n that is the 45° projection of the single axial load F_{tot}. The resulting contact area is an ellipse whose characteristics can be calculated using the elastic Hertz theory. For unique loading direction, only one side of the thread works because of axial backlash.

2.2. Dynamic features

The overall motion is similar to that of a planetary gear train: the rotation of the screw drives the orbital motion of the rollers. The rollers are synchronized with spur gears at their tops and ring gears at the top of the nut. The rollers threads are rolling on those of the nut and the screw.

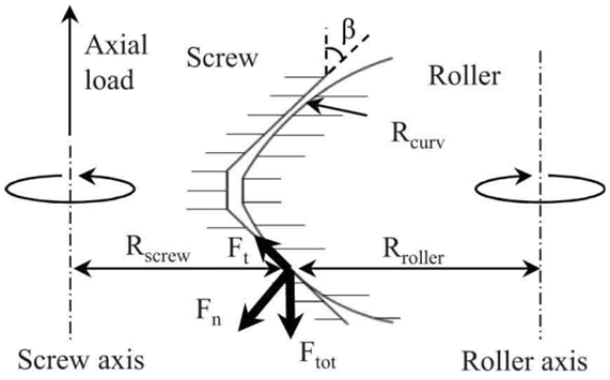

Fig. 2 Screw / Roller single contact features

Since the nut and the screw have the same pitch Eq. (1) and different diameter in order to house the rollers Eq. (2), their two threads have different helix angles Eq. (3). Besides, the rollers must have the same helix angle as the nut to prevent them from axial migration as they roll into the nut Eq.(4) [4]. Thus, the roller helix angle cannot also be equal to that of the screw Eq. (5).

$$p_{nut} = p_{screw} \tag{1}$$

$$R_{nut} = R_{screw} + 2 \times R_{roller} \tag{2}$$

$$p_i = 2\pi \times R_i \times \tan \alpha_i \tag{3}$$

$$\alpha_{nut} = \alpha_{roller} \tag{4}$$

$$\alpha_{screw} \neq \alpha_{roller} \tag{5}$$

This difference results in an overall axial sliding component, perpendicular to the rolling direction, which can be expressed with a slip ratio (τ) given by Eq. (6).

$$\tau = \frac{V_{sliding}}{V_{rolling}} \tag{6}$$

A complete analysis of the PRS is provided by Velinsky *et al.* [3]. This approach gives the global axial sliding speed considering the angular speed of the screw Eq. (7) where ω_{screw} is the angular speed of the screw.

$$V_{ax.sliding} = R_{screw} \cdot \omega_{screw} \cdot \tan \alpha_{screw} \tag{7}$$

This expression reveals that the axial extension of the screw is only made of sliding at each single contact. Then, the basic principle of the system is to combine this sliding to a rolling component, in a proportion which is defined by the slip ratio. For tribology matters, it is interesting to express the rolling speed and the slip ratio at each contact.

The rolling speed is defined as the angular speed of the rollers as they roll on the screw profile. It is calculated with Eq. (8).

$$V_{rolling} = \frac{R_{screw} + 2 \times R_{roller}}{2 \times \left(R_{screw} + R_{roller} \right)} \cdot R_{screw} \cdot \omega_{screw} \tag{8}$$

The creep ratio can be calculated by considering the gap between the helix angle of the screw, and the helix angle of the rollers which is generally oriented in the opposite direction. Fig. 3 illustrates this gap with exaggerated angles:

The rollers move in the orbital direction at the speed of $V_{rolling}$ To stay on the screw pitch line, the contact must slide in the axial direction at the speed $V_{ax.sliding}$ given by Eq. (9).

$$V_{ax.sliding} = V_{rolling} \cdot \left(\tan \alpha_{screw} + \tan \alpha_{roller} \right) \tag{9}$$

Due to PRS geometry characteristics, this expression of Eq. (9) gives the same results as the previous expression of $V_{ax.sliding}$ Eq. (7). Since the contacting threads are tilted from the axis to an angle β, the actual sliding speed and slip ratio at the contact point and the creep ratio are given by Eq. (10) and Eq. (11).

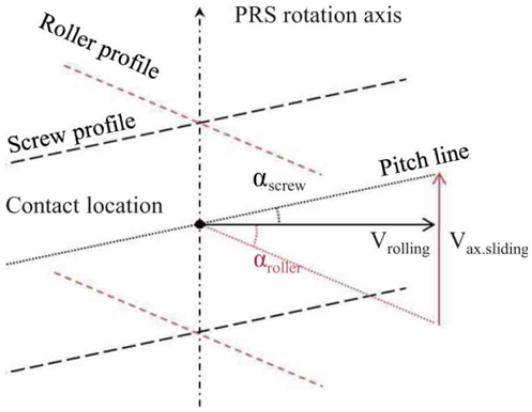

Fig. 3 Axial schematic view of the PRS contact

$$V_{sliding} = V_{rolling} \cdot \left(\tan\alpha_{screw} + \tan\alpha_{roller}\right) \cdot \cos\beta \qquad (10)$$

$$\tau = \frac{V_{sliding}}{V_{rolling}} = \left(\tan\alpha_{screw} + \tan\alpha_{roller}\right) \cdot \cos\beta \qquad (11)$$

The creep ratio and the rolling speed are directly related to the PRS design: for small pitches PRS, helix angles are smaller than for large pitches PRS, but applied speeds are usually higher. Then, the wear behavior would be different from one design to another. Typically, the creep may vary from 5 to 10%. Finally, since the contact is not punctual and is tilted from the rotation axis, the constant sliding lines inside the contact describe a class of circles whose centers may or may not lie within the contact area. This phenomenon is referred to as spin [8]. In the small pitch PRS considered in the present study, the width of the contact area is negligible compared to the pitch radius, so that the sliding lines can be considered as parallel, and the spin effect is neglected.

Some orbital sliding can also occur when there is a pitch mismatch between the gears and the thread. It results in a slight axial migration of the rollers [2]. This component is due to manufacturing errors, and is not discussed in this paper. Finally, slip can also arise due to the difference between the two surfaces curvatures. It has been suggested that this micro-slip can be sufficient to generate adhesive wear, and responsible for the rolling resisting moment [1,5].

The single contacts that carry the load in the PRS can then be described as ellipsoid on flat contacts, with a rolling-sliding motion. Since the spin effect due to the tilted contact is second order, they can be assimilated to a more common rolling contact with rotation axis parallel to the contact area, and subjected to the normal load F_n.

Thus, it is similar to the wheel/rail contact or gear tooth contact [6,7], but with a sliding motion perpendicular to the rolling direction [8,9].

3. Experimental methods

3.1. Rolling-sliding tribometer and samples

The PRS single contact is difficult to reproduce experimentally. But it can be reasonably assimilated to the contact of a curved body on a flat surface, with rolling and sliding. A test rig has been developed to simulate this simplified configuration and then study the damage induced by the rolling-sliding motion. It uses a torus applied on a flat disc (Fig. 4), which represent respectively the roller and the screw profiles. A given PRS of small pitch (p_{screw} = 2.5 mm) has been chosen as a reference for the design of the two specimens. The aim is to obtain the same characteristics of contact: ellipse size and contact pressure for a given load, same materials and lubrication.

The external radius of the torus is 10 mm. It corresponds to the pitch radius R_r of the PRS roller. The radius of curvature is set to 1.5 mm, equal to the roller curved profile.

The roller is mounted on a small shaft that rolls freely on small ball bearings inside a holder. The holder is fixed to a shaft that loads the assembly on the rotating disc (Fig. 5).

The axial shift Δ between the roller axis and the disc axis perpendicularly to the radius of the disc is controlled with precision and creates a transverse sliding component (Fig. 6). As a result, it generates a tangential force F_t. Tangential force and rolling speed are measured and recorded. The creep ratio τ is defined by Eq. (12) and Δ is calculated with Eq. (13), where R is the radius of

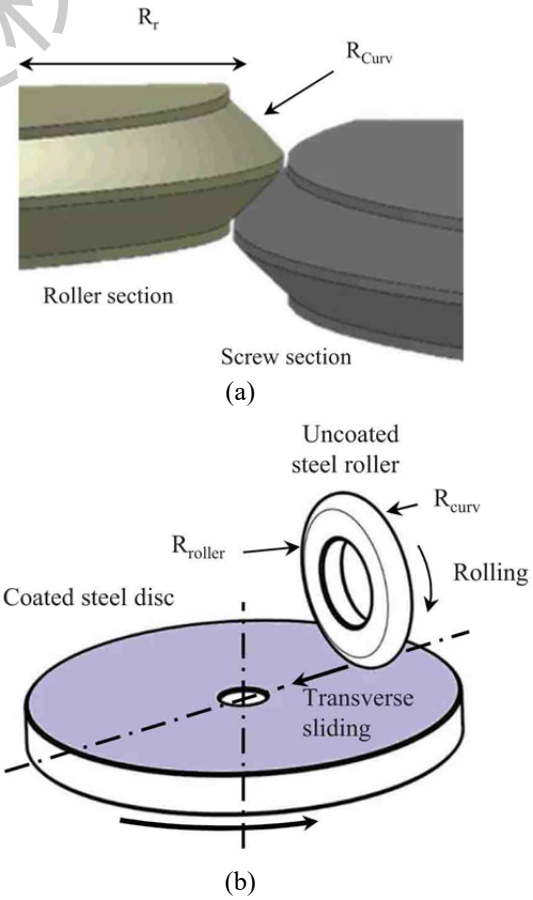

Fig. 4 Standard configuration of the simulated contact (a) PRS screw/roller contact (b) test rig contact

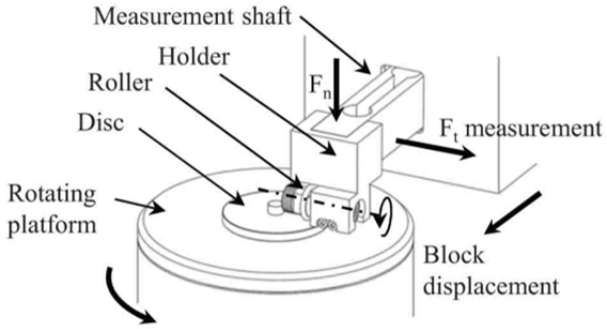

Fig. 5 Tribometer

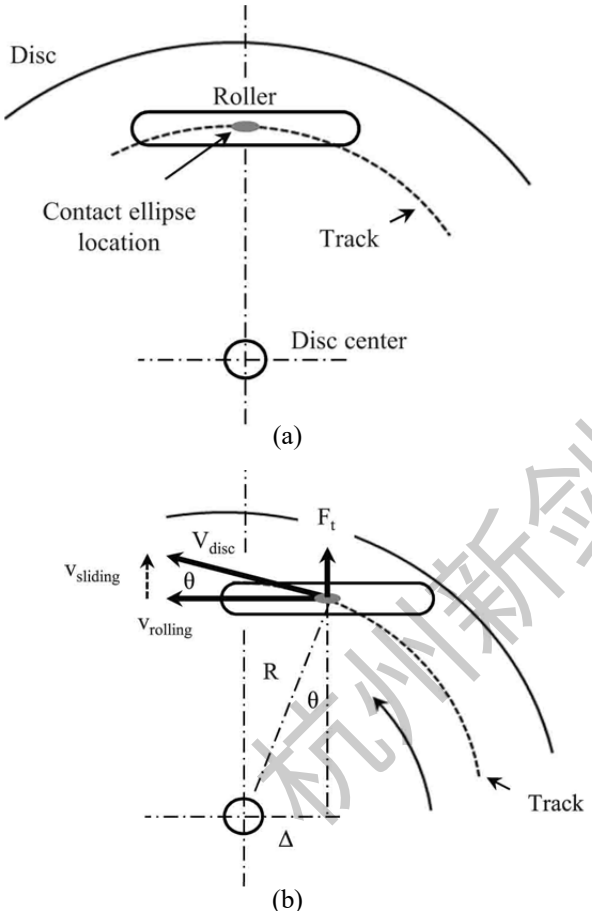

Fig. 6 Generation of the transverse sliding component (a) Top view of pure rolling position $\Delta = 0$ (b) Top view of rolling-sliding position $\Delta \neq 0$

track on the disc.

$$\tau = \frac{V_{sliding}}{V_{rolling}} = \tan\theta \quad (12)$$

$$\Delta = R \cdot \sin\theta = R \cdot \sin\left(\operatorname{atan}\tau\right) \quad (13)$$

On this specific tribometer, one cycle is defined as one rotation of the disc, which corresponds to 3 rotations of the roller. A microscope and a camera have been added to the tribometer: during the tests, the rotation is stopped at chosen cycle intervals, and pictures of one segment of the track on the disc are taken. Then, it is possible to make a frame by frame movie of the evolution of the track at the end of the test. That apparatus does not provide an in-situ observation of the contact, but it is suitable to analyze progressive phenomena such as cracking and abrasion.

3.2. Materials and coating

The materials are high hardness martensitic stainless steels (≥ 58 HRc), similar to those of the PRS components, and the surfaces are polished (R_a < 0.05 µm).

After polishing, the disc surface is coated with a WC/C industrial coating with a thickness of 3 µm. This coating is made of three layers: one upper layer of superlattice structure (WC/C), a middle layer of tungsten carbide WC, and an interface chromium layer for adhesion with the substrate. This type of coating is supposed to be suitable for the highly stressed contact points thanks to the multilayer structure of the WC/C upper material [10].

3.3. Test conditions

Most of the tests are carried out with an uncoated steel roller and a coated disc (Fig. 4), which is the configuration that is most likely to appear on real parts. Table 1 summarizes the wear test conditions of the roller-disk contact on the tribometer, in order to simulate one single contact between the roller and the screw in the PRS. All tests are performed at room temperature (22°C) and in dry conditions.

4. Results and discussion

4.1. Typical friction stages

The solid line of Fig. 7(a) shows the typical evolution of the friction coefficient in standard configuration, and Fig. 8 shows pictures from the frame by frame video of the test. During the first cycles, Fig. 7(b), the friction coefficient increases rapidly to 0.25-0.3, and then drops slowly to 0.1 during 5×10^4 to 1×10^5 cycles. It stabilizes around 0.1 and start to increase again from a number of cycles that depends on the contact conditions. That final increase corresponds to the total wear of the coating.

Table 1 Test conditions and contact parameters

Normal load F_n	80 - 280 N
Maximum Hertz pressure p_{max}	2500 - 4000 MPa
Ellipse size	a = 0.2 - 0.3 mm b = 0.06 - 0.1 mm
Side-slip ratio τ	0 – 10 %
Contact rolling speed $V_{rolling}$	0.5 – 2 m.s^{-1}

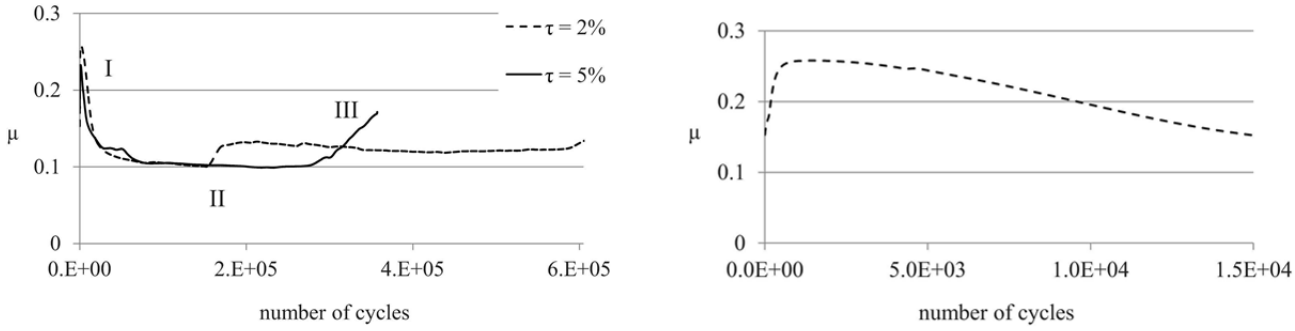

(a) (b)

Fig. 7 Typical evolutions of the friction coefficient, F_n = 80 N (p_{max} = 2.5 GPa), $V_{rolling}$ = 1 m·s^{-1} (a) for two values of side-slip ratio (2 and 5%) (I) running-in (II) nominal friction (III) under-layers abrasion (b) for a slip ratio of 2%, during the first cycles

4.2. Running-in stage and nominal friction stage

During the first cycles, the coated surface is progressively smoothed (Fig. 8(a,b)). Some tests carried out in the opposite coating configuration, i.e. with a coated roller and an uncoated steel disc, reveal the formation of a granular transfer film on the uncoated surface (Fig. 9) that matches the description of Holmberg *et al*. [10]. EDX analysis shows a high content of tungsten and oxides that suggests that the film is built by adhesion phenomena. The duration of its growth to 1-2 μm thick corresponds to the decrease of the friction coefficient to 0.1. The frame by frame video shows the continuous formation and wear of the film, suggesting that it acts as a lubricating third-body during all the nominal friction stage. Some tests have been carried out with coating on both surfaces, showing a slightly higher coefficient of friction (0.12) and no transfer film on the observation, that suggests that the film needs a metallic surface to fix on.

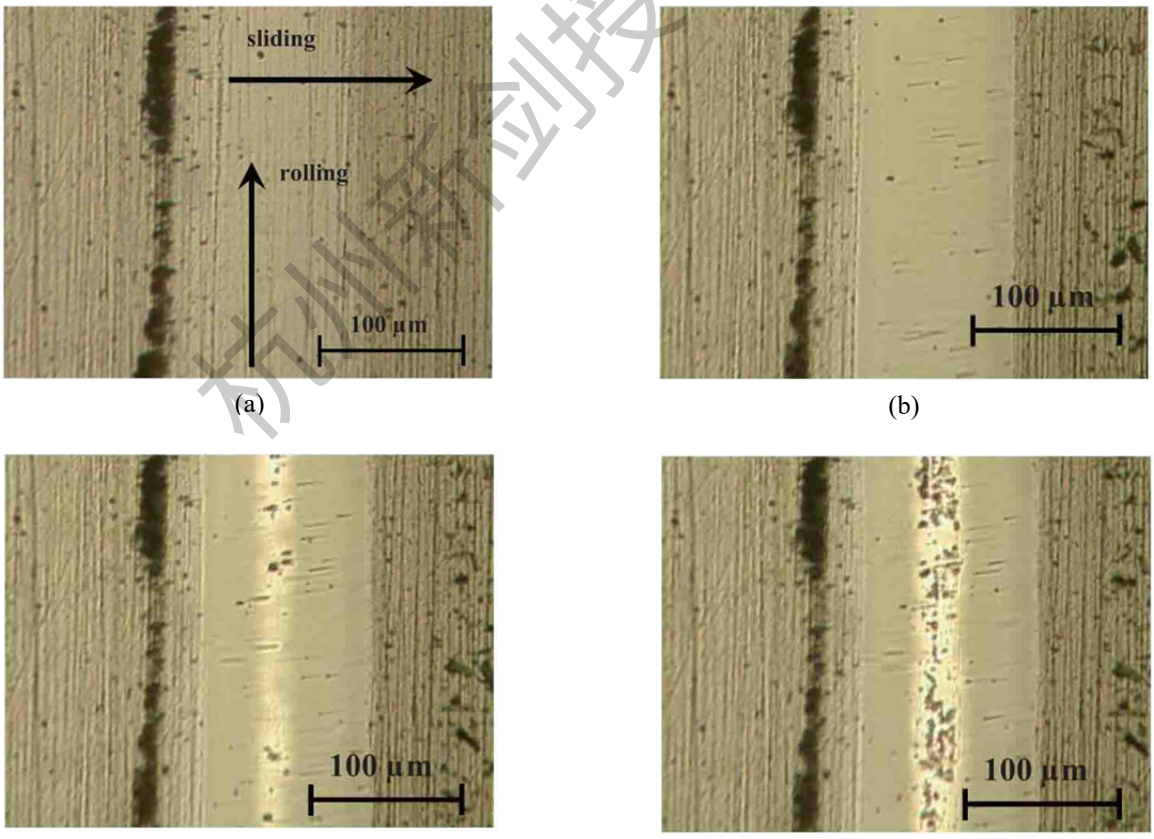

(a) (b)

(c) (d)

Fig. 8 Evolution of the coated track (F_n = 80 N, τ = 5 %, $V_{rolling}$ = 1 m·s^{-1}) (a) 1 × 10^3 cycles (b) 2.5 × 10^5 cycles (c) 3 × 10^5 cycles (d) 3.5 × 10^5 cycles

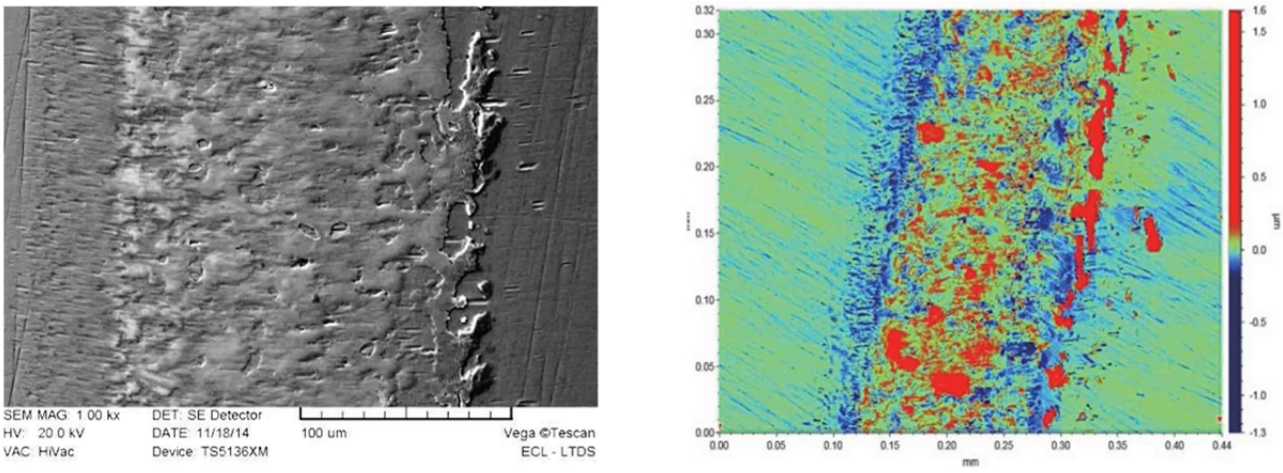

(a) (b)

Fig. 9 Transfer film observation (a) SEM (b) interferometry

4.3. Abrasive wear

At a time that depends on the contact conditions, the friction coefficient increases again and a clear zone starts to appear on the center of the coated track (Fig. 8(c,d)) with black particles that are continuously transferred and removed on it. EDX analysis reveals a lower content of carbon and a higher content of tungsten on the clear zone suggesting that it corresponds to the WC under-layer. The black particles have the same chemical composition as the transfer film, suggesting that it is re-transferred from the uncoated surface to the coated one. As the test proceeds, the clear zone becomes larger, and chromium and iron finally appear. Then, friction coefficient of 0.3 to 0.5 is reached. This progressive removal of the coating may be closely linked to the equilibrium of the constant formation and removal of the transfer film on the steel counter-body. The wear rate can be quantified by measuring the worn section S of the coated track after or during the tests. Fig. 10(a) corresponds to the worn section measurement of the segment of the track from Fig. 8(c). It reveals a wear depth that is almost equivalent to the coating thickness (3 µm). Measurements from many other tests in various conditions (Table. 1) bring out that the evolution of the worn section as a function of the product of the normal force by the sliding distance ($N_{cycles} \cdot \tau$) is quite linear (Fig. 10(b)). It also appears that the rate of this evolution is appreciably higher when the normal load F_n is higher. Then the abrasive wear of the WC/C coating seems to be partially coherent with the classic Archard wear law.

4.4. Fatigue wear

The dashed line of Fig. 7 corresponds to a test in the same contact conditions but with a low slip ratio (τ = 2%). The final increase of the friction coefficient appears much later since the abrasion speed is lower. But it also increases rapidly during the nominal friction stage (1.6×10^5 cycles), and frame by frame video shows that this corresponds to the cracking of the coating (Fig. 11(a)). The cracks are oriented in the rolling direction, i.e. perpendicular to the sliding direction, and they are localized at the exit side of the sliding. These observation are in accordance with the Hamilton *et al*. [11] description of the tangential stresses under a circular sliding contact, where the rear of the contact undergoes traction stresses. Fig. 11(b) shows a cross section of a cracked sample, tilted at 45°. The cracks seem to stop at the interface, without propagating

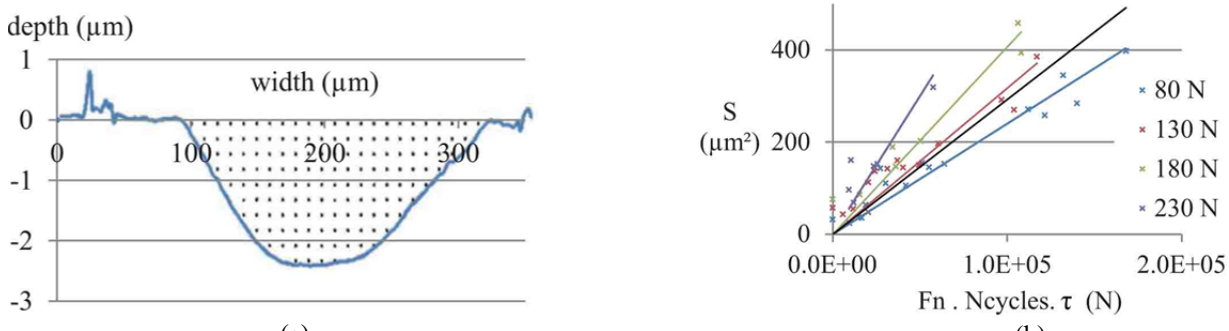

(a) (b)

Fig. 10 Worn section of the coated track on the disc (a) worn section profile (3×10^5 cycles) (b) worn section evolution for various normal loads

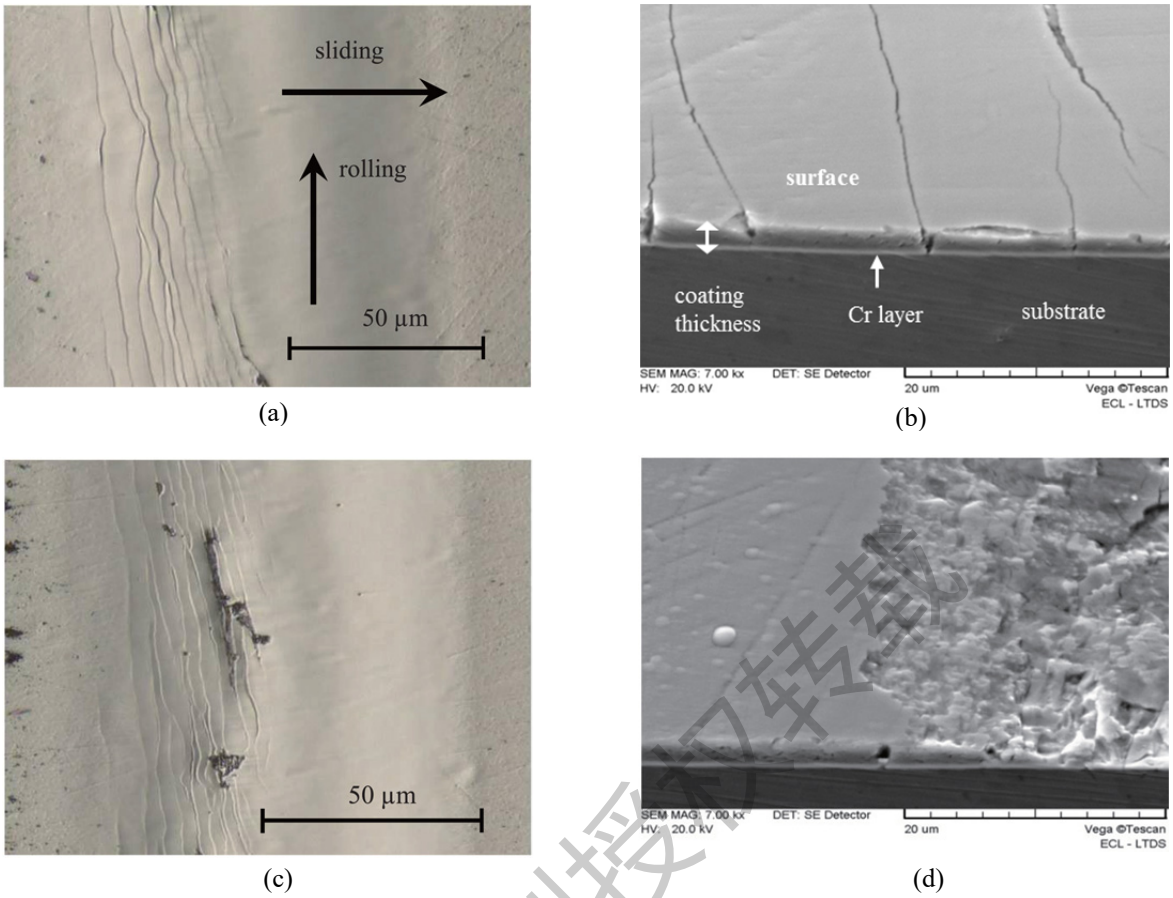

Fig. 11 Observation of the cracked coating (a) observation of the cracks disposition (b) SEM cross-section (45° tilt) of the cracked surface (c) observation of the spalled surface (d) SEM cross section (45° tilt) of the spalled surface

neither in the steel substrate, nor at the interface, which may suggest the relatively high toughness of these materials. For sufficient shear stresses, that is for high slip ratios ($\tau > 5\%$) and high contact pressures ($p_{max} > 3$ GPa), the cracks lead to a partial delamination (Fig. 11(c)). This appears to be cohesive delamination, i. e. inside the coating structure rather than at the interface. Once the coating is partially spalled, or only cracked, the phenomena tends to stop and the frame by frame video reveals a progressive smoothening of the damaged coating, which corresponds to the stabilization of the friction coefficient (Fig. 7, dashed line, from 2×10^5 to 4×10^5 cycles).

4.5. Wear mode maps

The mild polishing wear and the cohesive delamination have been identified in the literature as the two main damage modes of the WC/C coating under rolling-sliding conditions [12,13]. In the present contact conditions, the third-body polishing wear appears to be the main damage mode since it is progressive and quite unavoidable. Besides, it is predictable and can be monitored. On the contrary, the fatigue damage is more difficult to predict and to quantify than the abrasive wear. It does not seem to be heavily detrimental for the contact, since it does not lead to a global failure, but it causes a quick and quite random increase of the friction and an emission of potentially abrasive wear debris from the spalled coating. Then it can be considered as a parasite damage mode that should be avoided. The multiple experiments, which are stopped after the total removal of the coating, revealed that cracking may or may not occur in the meantime, depending on the contact conditions. They also brought out that in the studied range (Table 1), the rolling speed (and hence the sliding speed) does not influence the type of damage. A wear mode map (Fig. 12) has been established based on these experiments to present the areas of contact pressure and slip ratios in which each damage mode is predominant. The test duration before the total wear of the coating depends on the slip ratio magnitude and the normal load, then the map does not take into account the number of cycles. Several domains have been identified:

- I. For low slip ratios ($\tau < 1\%$), the shear stresses are not sufficient to generate cracks, and the observation only reveals a soft and very slow abrasion, even at high contact pressure, until total removal of the coating.

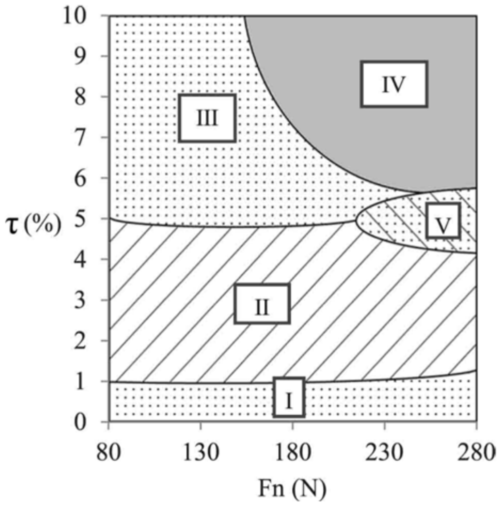

Fig. 12 Damage mode map of WC/C coating in rolling-sliding motion

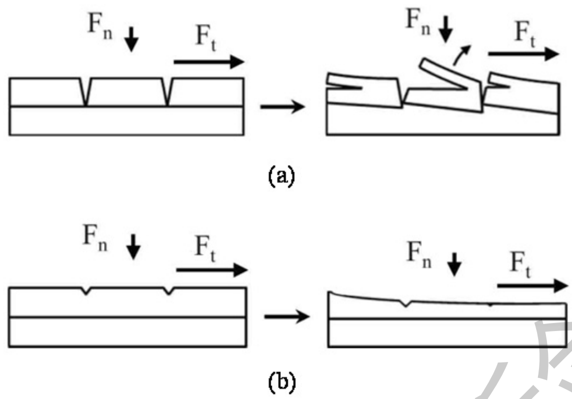

Fig. 13 Illustration of the two main damage mode (a) cracks and cohesive delamination (II) (b) abrasive wear (III)

- II. For higher slip ratios ($1\% < \tau < 5\%$), the coating may crack and delaminate (Fig. 11 & Fig. 13(II)) before the total removal of the coating.
- III. For even higher slip ratios ($5\% < \tau < 10\%$), the abrasion speed is too important compared to propagation speed of the cracks (Fig. 13(III)). Then, cracks do not appear before total abrasion of the coating. This competition is well illustrated by Fig. 7 for two tests in same conditions and different slip ratios.
- IV. For very high stress conditions ($p_{max} > 3.5$ GPa (F_n = 180 N), $\tau > 6\%$), a global spalling of the coating occurs during the very first cycles and the friction coefficient increases to chaotic values around 0.3 with no further decrease. In that case, the tests are stopped soon after the beginning.
- V. A mixed area where cracking and spalling occurs rapidly and almost simultaneously has also been observed between area II and IV.

5. Conclusions

This work investigates the tribological behavior of the contact at the screw/roller and nut/roller interfaces of the PRS mechanisms. A simple analysis that describes the contact characteristics has been provided. As a result, the contact can be considered as an ellipsoid on flat contact with a rolling component, and a sliding component perpendicular to the rolling direction. This makes the PRS contact much singular among usual bearing mechanisms. The contact parameters such as normal load, rolling speed and slip ratio are derived. The slip ratio is related to the helix angles, which are directly linked to the pitch of the screw. Then, the magnitude of slip in each single contacts is proportional to the pitch size.

A specific apparatus has been developed to reproduce the simplified PRS contact features: it simulates the screw/roller and nut/roller interfaces with a torus roller rolling and sliding on a disc. Input parameters such as normal load, rolling speed and creep ratio are controlled, so that the static and dynamic features of the contact ellipse in the laboratory test are representative of the contact in one reference PRS used in industry. The disc samples are coated with a WC/C hard coating which is supposed to be adapted to these contact conditions.

Tests have been performed in dry conditions. They bring out the formation of a transfer film on the coated surface, which is supposed to be responsible for the drop of the friction coefficient from 0.3 to 0.1. However, the duration of this running-in stage is significant compared to the duration of the nominal friction stage before total abrasion. That means that the coating needs many cycles before being efficient. Deposition of WC/C coating on both surfaces does not improve the running-in since the lubricating transfer film cannot fix on the surfaces.

Two damage modes have been identified for sufficiently low shear stresses: abrasion and fatigue. A competition between the two has been observed, and has been illustrated by a wear map. It shows that cracks may or may not occur depending on the magnitude of the slip ratio: for small slip ratios, the total abrasion of the coating needs a high number of cycles which is sufficient to generate cracks. On the contrary, for high slip ratios, the quick removal of the coating material limits the propagation of cracks inside it. These conclusions show that large pitch screws, that include a high slip ratio, would be safer than small pitch screws since the coating should only be subject to abrasion.

Nomenclature

i screw, nut or roller

F_{tot} axial load on a single contact (N) $= \dfrac{\text{total axial load}}{\text{number of contact points}}$

F_n normal force (N) $= \dfrac{F_{tot}}{\cos\beta}$

F_t	tangential friction force (N)
R_{curv}	roller profile radius of curvature (mm)
R_i	pitch radius of the component *i* (mm)
R	radius of the track on the disc (mm)
τ	creep ratio (= $V_{sliding}$ / $V_{rolling}$ = tan Θ)
Θ	slip angle (°)
Δ	axial shift on the test rig
p_i	pitch of the component *i* (mm)
α_i	helix angle of the component *i* (°)
β	tilt angle (°) generally equal to 45°
$V_{rolling}$	in-plane rolling speed of the PRS contact ($m \cdot s^{-1}$)
$V_{sliding}$	in-plane sliding speed of PRS the contact ($m \cdot s^{-1}$)
$V_{ax.sliding}$	axial sliding speed of the PRS contact ($m \cdot s^{-1}$)
V_{disc}	speed of the contact point on the disc ($m \cdot s^{-1}$)
$v_{rolling}$	speed of the contact point on the roller ($m \cdot s^{-1}$)
$v_{sliding}$	sliding speed of the roller sample ($m \cdot s^{-1}$)
p_{max}	maximum Hertz pressure (MPa)

References

[1] Halme, J. and Andersson, P., "Rolling Contact Fatigue and Wear Fundamentals for Rolling Bearing Diagnostics - State of the Art," Proc. Inst. Mech. Eng. Part J J. Eng. Tribol., 224, 4, 2010, 377-393.

[2] Jones, M. H. and Velinsky, S. A., "Kinematics of Roller Migration in the Planetary Roller Screw Mechanism," J. Mech. Des., 134, 6, 2012, 061006-1-061006-6.

[3] Sokolov, P. A. and Blinov, D. S., "Promising Rotation-Translation Converters," Russ. Eng. Res., 28, 10, 2008, 949-956.

[4] Velinsky, S. A., Chu, B. and Lasky, T., "Kinematics and Efficiency Analysis of the Planetary Roller Screw Mechanism," J. Mech. Des., 131, 1, 2009, 011016-1-011016-8.

[5] Johnson, K. L., "Contact Mechanics," Cambridge University Press, Cambridge, 1985.

[6] Ayasse, J. and Chollet, H., "Handbook of Railway Vehicle Dynamics," CRC Press, 2006, 85-120.

[7] Olofsson, U. and Lewis, R., "Handbook of Railway Vehicle Dynamics," CRC Press, 2006, 121-138.

[8] Monk-Steel, A. D. and Thompson, D. J., "An Investigation into the Influence of Longitudinal Creepage on Railway Squeal Noise due to Lateral Creepage," J. Sound Vib., 293, 3-5, 2006, 766-776.

[9] Thompson, D. and Jones, C., "Handbook of Railway Vehicle Dynamics," CRC Press, 2006, 280-322.

[10] Holmberg, K. and Matthews, A., "Coatings Tribology-Contact Mechanisms and Surface Design," Tribol. Int., 31, 1-3, 1998, 107-120.

[11] Hamilton, G. M. and Goodman, L. E., "The Stress Field Created by a Circular Sliding Contact," J. Appl. Mech., 33, 2, 1966, 371-376.

[12] Yonekura, D. and Chittenden, R. J., "Wear Mechanisms of Steel Roller Bearings Protected by Thin, Hard and Low Friction Coatings," Wear, 259, 1-6, 2005, 779-788.

[13] Gold, P. W. and Loos, J., "Wear Resistance of PVD-Coatings in Roller Bearings," Wear, 253, 3-4, 2002, 465-472.